See related commentary on pg 940

ORIGINAL ARTICLE

Aberrant Connexin26 Hemichannels Underlying Keratitis–Ichthyosis–Deafness Syndrome Are Potently Inhibited by Mefloquine

Noah A. Levit[1], Caterina Sellitto[1], Hong-Zhan Wang[1], Leping Li[1], Miduturu Srinivas[2], Peter R. Brink[1] and Thomas W. White[1]

Keratitis–ichthyosis–deafness (KID) syndrome is an ectodermal dysplasia caused by dominant mutations of connexin26 (Cx26). Loss of Cx26 function causes nonsyndromic sensorineural deafness, without consequence in the epidermis. Functional analyses have revealed that a majority of KID-causing mutations confer a novel expansion of hemichannel activity, mediated by connexin channels in a nonjunctional configuration. Inappropriate Cx26 hemichannel opening is hypothesized to compromise keratinocyte integrity and epidermal homeostasis. Pharmacological modulators of Cx26 are needed to assess the pathomechanistic involvement of hemichannels in the development of hyperkeratosis in KID syndrome. We have used electrophysiological assays to evaluate small-molecule analogs of quinine for suppressive effects on aberrant hemichannel currents elicited by KID mutations. Here, we show that mefloquine (MFQ) inhibits several mutant hemichannel forms implicated in KID syndrome when expressed in *Xenopus laevis* oocytes ($IC_{50} \sim 16\,\mu M$), using an extracellular divalent cation, zinc (Zn^{++}), as a nonspecific positive control for comparison ($IC_{50} \sim 3\,\mu M$). Furthermore, we used freshly isolated transgenic keratinocytes to show that micromolar concentrations of MFQ attenuated increased macroscopic membrane currents in primary mouse keratinocytes expressing human Cx26-G45E, a mutation that causes a lethal form of KID syndrome.

Journal of Investigative Dermatology (2015) **135,** 1033–1042; doi:10.1038/jid.2014.408; published online 16 October 2014

INTRODUCTION

Connexin genes encode gap junctions, which establish a direct signaling pathway between virtually all contacting cell types (Goodenough and Paul, 2009). Gap junctions are clusters of intercellular channels that enable exchange of ions, second messengers, and small metabolites to mediate coordinated functions within tissues (Bruzzone *et al.*, 1996). Connexins are tetraspan membrane proteins that form oligomers, termed ''hemichannels,'' which dock in pairs to couple adjacent cells. Several connexins are now appreciated to produce functioning hemichannels in a nonjunctional configuration with uncertain physiological relevance (DeVries and Schwartz, 1992; Ebihara and Steiner, 1993; Malchow *et al.*, 1993).

Connexin mutations cause human hereditary diseases (Pfenniger *et al.*, 2011). Mutations in connexin26 (Cx26 or *GJB2*) are the major cause of nonsyndromic deafness, as well as syndromic hearing loss that presents in conjunction with skin disorders such as keratitis–ichthyosis–deafness (KID) syndrome (Scott and Kelsell, 2011). Cx26 gap-junction channels were found to be either partially or completely nonfunctional for a majority of autosomal recessive mutations leading to nonsyndromic deafness (Zhao *et al.*, 2006). Conversely, clinical scenarios involving skin pathology are transmitted through dominant Cx26 mutations that are suspected to confer novel channel activities (Richard, 2005).

KID syndrome is characterized by profound hearing loss, vascularizing keratitis, and extensive erythrokeratoderma (Skinner *et al.*, 1981; Richard *et al.*, 2002). KID patients suffer recurrent infections that can precipitate lethal septicemia (Haruna *et al.*, 2010; Sbidian *et al.*, 2010). Additional features include the follicular occlusion triad (dissecting folliculitis, hidradenitis suppurativa, and cystic acne) and malignant transformation of hyperkeratotic plaques to squamous cell carcinoma (Montgomery *et al.*, 2004; Mazereeuw-Hautier *et al.*, 2007). A total of 10 distinct Cx26 missense mutations are associated with KID syndrome, and electrophysiological analysis has identified a pattern of increased hemichannel behavior shared by many of them. Specifically, Cx26-G45E, -D50N, -A40V, -N14K, -G12R, -A88V, and -D50A induce significantly greater hemichannel activity than wild-type (WT) channels under

[1]*Department of Physiology and Biophysics, Stony Brook University, Stony Brook, New York, USA and* [2]*Department of Biological and Vision Sciences, SUNY College of Optometry, New York, USA*

Correspondence: Thomas W. White, Department of Physiology and Biophysics, Stony Brook University, T5-147, Basic Science Tower Stony Brook, New York 11794-8661, USA. E-mail: thomas.white@stonybrook.edu

Abbreviations: KID, keratitis–ichthyosis–deafness; Cx26, connexin26; MFQ, mefloquine

Received 29 May 2014; revised 2 August 2014; accepted 4 September 2014; accepted article preview online 17 September 2014; published online 16 October 2014

the same experimental conditions (Montgomery *et al.*, 2004; Stong *et al.*, 2006; Gerido *et al.*, 2007; Lee *et al.*, 2009; Sanchez *et al.*, 2010; Donnelly *et al.*, 2012; Mhaske *et al.*, 2013). Constitutively active or ''leaky'' hemichannels are predicted to cause ionic imbalances and interrupt differentiating keratinocytes with injurious consequences for the epidermis.

A pathogenic role for dysregulated hemichannels in KID syndrome awaits definitive demonstration. Pharmacological tools to modulate Cx26 are needed to assess the pathogenic role for hemichannels in KID syndrome. Previous drug screens have implemented dye transfer methods with automated fluorescence microscopy imaging to identify candidate compounds (Li *et al.*, 2003; Picoli *et al.*, 2012). However, these studies could not discriminate between direct and indirect inhibitor actions, and they failed to account for the possibility of differential drug affinities for mutant channel forms that are important in human disease. Using two different electrophysiological assays, we show quantitative evaluation of prospective small-molecule inhibitors of mutant Cx26 hemichannels present in KID syndrome, and include an extracellular divalent cation, zinc (Zn^{++}), for comparison. Mefloquine (MFQ) emerged as a leading candidate among five tested compounds selected for affinity to connexin targets. Our results indicate that micromolar doses of MFQ potently attenuate Cx26 hemichannel currents associated with the majority of KID mutations and show that it is particularly well positioned for testing in a transgenic mouse model of the lethal form of the disease.

RESULTS AND DISCUSSION

Increased hemichannel activity associated with KID-causing Cx26 mutations

Previous reports have described increases in hemichannel functionality as a common feature shared by Cx26 mutations linked to KID syndrome (Montgomery *et al.*, 2004; Stong *et al.*, 2006; Gerido *et al.*, 2007; Lee *et al.*, 2009; Sanchez *et al.*, 2010; Donnelly *et al.*, 2012; Mhaske *et al.*, 2013). Before pursuing inhibitor studies, we quantified membrane currents in single *Xenopus* oocytes expressing Cx26-G45E, -D50N, -A40V, -N14K, -G12R, -D50A, and -A88V, with Cx26-WT- and water-injected control cells. KID syndrome mutations result from single amino-acid substitutions that localize to the Cx26 N terminus and first extracellular loop, with the exception of A88V, which appears in the second transmembrane domain. To assay membrane current, cells were voltage-clamped at −40 mV and subjected to a series of depolarizing transmembrane voltages (Figure 1a). Negligible membrane current was recorded from oocytes injected with H_2O for voltages between −30 and +60 mV. WT Cx26 hemichannels favored a low open-probability resting state with outward current induced by membrane depolarization and an approximately linear current–voltage relationship, as previously demonstrated (Ripps *et al.*, 2004; Gonzalez *et al.*, 2006). The Cx26-G45E, -D50N, -A40V, -N14K, -G12R, -D50A, and -A88V mutants displayed increased outward currents relative to H_2O or Cx26-WT-injected cells. At the largest voltage tested, Cx26-WT hemichannels passed maximal currents of 0.5–1.5 μA, and the recorded conductance was 10.5-, 7.5-, 8-, 8-, 4.5-, 4-, and 8-fold higher in Cx26-G45E, -D50N, -A40V, -N14K, -G12R, -D50A, and -A88V, respectively. Western blotting of cell lysates for total Cx26 content eliminated the possibility that the different magnitudes of membrane current arose from unequal levels of protein expression (Figure 1b). The Cx26 band intensity was approximately equal across the seven mutant groups, and within ±10% of the expression level of Cx26-WT when normalized to β-actin.

In vitro screening of quinine analogs for inhibitory efficacy on Cx26-G45E and Cx26-D50N hemichannels

Molecules that are therapeutically classified as antimalarial agents have been recognized to suppress hemichannel currents by direct action on connexin subunits, and partial-selectivity properties are conferred to these compounds by differences in affinities for connexin subtypes (Srinivas *et al.*, 2001; Cruikshank *et al.*, 2004; Rubinos *et al.*, 2012). Inhibitor studies involving MFQ have focused on connexin50 and connexin36, in the context of their roles as gap-junction proteins that couple lens epithelial cells and neurons, respectively (Cruikshank *et al.*, 2004). The ability of MFQ to modulate Cx26 channel activity had received only cursory examination and only with regard to WT junctional communication. We screened MFQ and four related derivatives (QU020, QU021, QU022, and QU026) for inhibitory capacity against dysregulated hemichannels resulting from two Cx26 mutations associated with the KID syndrome. Cx26-G45E causes a lethal form of KID syndrome (Janecke *et al.*, 2005; Griffith *et al.*, 2006; Jonard *et al.*, 2008) and is characterized by robust hemichannel activity that represents the most significant deviation from WT channel behavior (Gerido *et al.*, 2007). Cx26-D50N is the most commonly reported mutation in cases of KID syndrome. Drug screening was performed by perfusion of candidate inhibitors during voltage-clamp recording of Cx26-G45E (Figure 2a) and Cx26-D50N (Figure 2b) hemichannel currents in single *Xenopus* oocytes. Sequential depolarizing +50-mV pulses stimulated repeated channel opening and consistent bursts of whole-cell membrane current. Inhibitor effects were evaluated by exchange of the bathing medium for a segment of each recording (Figure 2, left). At a drug concentration of 30 μM, QU022 displayed unimpressive inhibition of membrane currents (<20% reduction) for both Cx26-G45E and Cx26-D50N. QU022 lacks the aliphatic piperidine ring present in MFQ and also substitutes a $–CCl_3$ group for the $–CF_3$ found on the quinolone ring, representing the most dissimilar molecule to MFQ tested. QU020 also failed to produce any marked suppression of Cx26-G45E hemichannels (25 ± 14%), but it was twice as effective when tested on Cx26-D50N hemichannels (49 ± 7.3%). QU021 performed at a similar level, approximately halving membrane currents passed by both mutant channels (52 ± 7.8% and 43 ± 12% for Cx26-G45E and -D50N, respectively). MFQ and QU026 elicited the most striking diminution in membrane currents recorded from single cells expressing either Cx26-G45E (70 ± 17% for 30 μM MFQ and 59 ± 13% for 30 μM QU026; Figure 2a, right) or

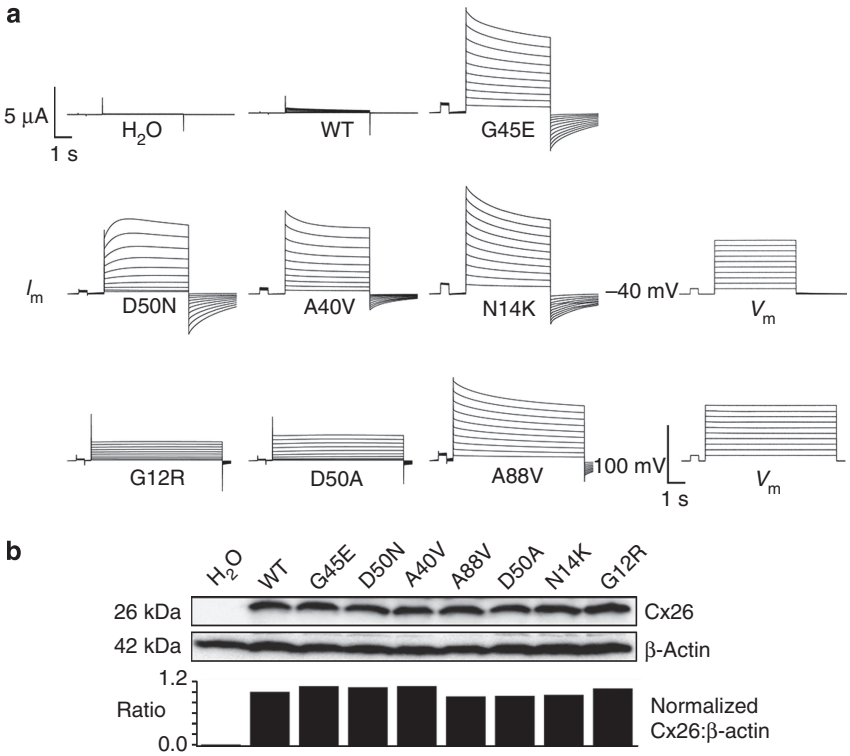

Figure 1. Cx26 mutations induced large hemichannel currents in *Xenopus* oocytes. (**a**) Cells were clamped at −40 mV and subjected to voltage pulses spanning −30 to +60 mV in 10-mV steps (V_m). H_2O-injected cells displayed negligible whole-cell membrane currents (I_m). Cx26-expressing oocytes all exhibited hemichannel currents; however, keratitis–ichthyosis–deafness syndrome mutations showed much larger currents than wild type (WT). (**b**) WT and mutant connexins are equivalently translated in *Xenopus* oocytes. Membrane extracts were probed with an antibody against Cx26. H_2O-injected controls did not express Cx26, whereas WT, Cx26-G45E, -D50N, -A40V, -A88V, -D50A, -N14K, and -G12R were detected. Blots were also probed with an antibody against β-actin; the normalized ratio of Cx26 to β-actin expression was quantified and found to be within ±10% of WT Cx26 for all mutations.

Cx26-D50N (69 ± 15% for 30 μM MFQ and 73 ± 11% for 30 μM QU026; Figure 2b, right). QU026 replaces the piperidine ring in MFQ with a third aromatic ring, but it includes no other structural deviation, possibly accounting for the parallel results. Two-CF_3 groups appear on the quinolone backbone of MFQ, QU020, QU021, and QU026—a feature that enhances the lipophilicity of these molecules. For this reason, it is possible that lipid-rich yolk granules that are abundant in stage V–VI oocytes may sequester a portion of the drug, effectively reducing the delivered dose and causing underreporting of potency in this system. Lipophilicity is, however, an appealing property of any drug considered for targeting epidermal proteins via topical delivery strategies. Given the status of MFQ as an FDA-approved drug with a history of safety and pharmacokinetic data, it was selected for further characterization.

MFQ attenuated hemichannel currents produced by five of seven KID-causing Cx26 mutations with concentration dependence and partial reversibility

We assessed the utility of MFQ for inhibiting the entire set of Cx26 mutations linked to KID syndrome and displaying high hemichannel activity. Three low micromolar concentrations were evaluated to probe for differences in sensitivity that may arise from unique biochemical or structural characteristics imparted by amino-acid substitutions. MFQ showed concentration-dependent reduction of Cx26-G45E hemichannel activity, with maximal suppression nearing total ablation of membrane currents (95.2% reduction at 100 μM). Raw recordings from three single cells tested at 10, 30, and 100 μM are shown to illustrate the instantaneous response of Cx26-G45E hemichannels to drug exposure and slow recovery of currents upon drug washout (Figure 3a). The magnitude of inhibition after 1.5 minutes of 10, 30, and 100 μM MFQ was 43 ± 8.0% (N = 5), 71 ± 7.9% (N = 5), and 89 ± 2.0% (N = 5), respectively (Figure 3b, extrapolated IC_{50} ~ 16 μM). Recovery of currents remained incomplete after 2.5 minutes of drug washout, ranging from 54 ± 5.0% (N = 5) to 84 ± 3.5% (N = 10) of initial current with an inverse correlation to concentration. Equivalent experiments were completed for Cx26-D50N, -A40V, -N14K, -G12R, -A88V, and -D50A, and summary data are provided for the average residual current in the presence of 10, 30, and 100 μM MFQ as a percentage of the pre-perfusion value (Figure 3c). None of the other mutants showed sensitivity comparable to Cx26-G45E, although Cx26-D50N, -A40V, -G12R, and -D50A hemichannel currents were all suppressed by 50% or better at 30 μM. In particular, Cx26-D50N and Cx26-G12R channels were >70% inactivated. Cx26-A88V and Cx26-N14K were refractory to inhibition by MFQ.

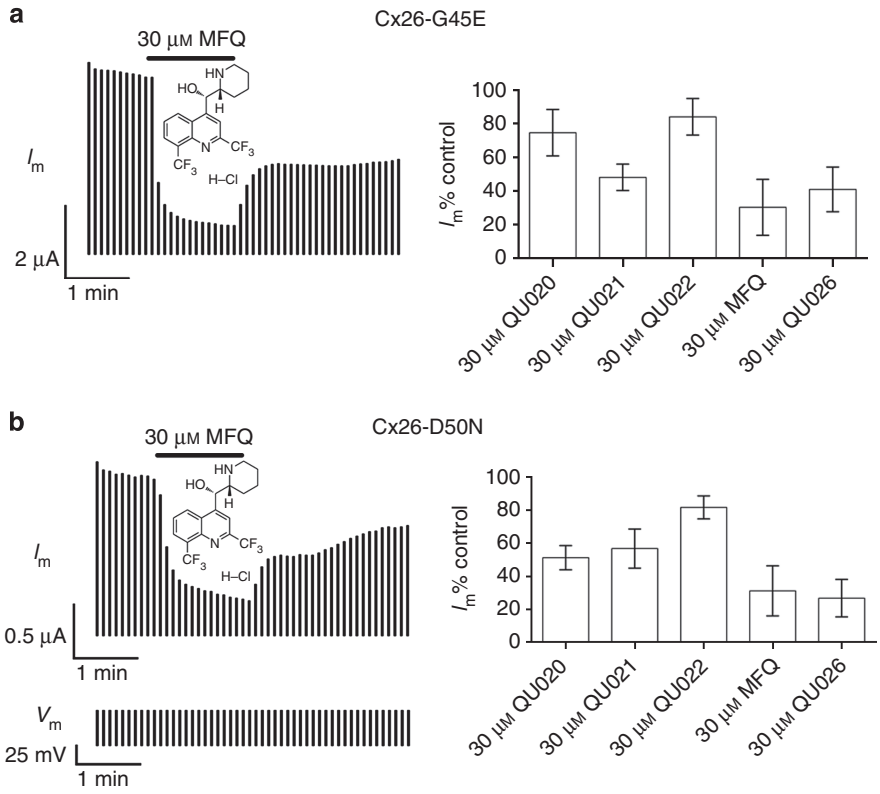

Figure 2. Mefloquine (MFQ) and quinine derivatives (QU0) suppressed (a) Cx26-G45E and (b) -D50N hemichannel currents in *Xenopus* oocytes. Single cells held at −40 mV were repeatedly pulsed with +50-mV depolarizations (V_m) and membrane current (I_m) was measured. Cells were exposed to 30 μM inhibitor for 90 seconds by switching perfusion solutions after 1 minute (left, shown for mefloquine). Inhibitors were washed out for 2.5 minutes, showing partial reversibility at the concentration tested. Summary data for inhibitors QU020, QU021, QU022, MFQ, and QU026 are shown as the mean residual instantaneous membrane current during 30 μM drug application as a percentage of the pre-drug value (right). MFQ and QU026 produced the greatest inhibition of Cx26-G45E and -D50N membrane currents. Data are the means ± SD.

Prior studies have examined the biophysical effects of connexin inhibitors with sufficient resolution to visualize single-channel gating events (Bukauskas and Peracchia, 1997; Weingart and Bukauskas, 1998; Srinivas and Spray, 2003). A consensus finding suggests that quinine analogs and MFQ affect channel activity by stimulating slow closure transitions called loop gating (Srinivas *et al.*, 2001; Rubinos *et al.*, 2012; Verselis and Srinivas, 2013). Structural components of the loop gating machinery include domains within the connexin N terminus and the first extracellular loop that form the hemichannel pore (Verselis *et al.*, 1994; Kronengold *et al.*, 2003; Maeda *et al.*, 2009; Tang *et al.*, 2009; Verselis *et al.*, 2009; Kronengold *et al.*, 2012). There is a clustering of most identified KID-causing Cx26 mutations to the protein N terminus and the first extracellular loop, suggesting that mutations that increase hemichannel activity may alter the intrinsic voltage-sensitive activation of slow gating, or impede conformational changes associated with the movement of the loops. MFQ may restore loop gating and thereby prevent leaking of unapposed hemichannels. The inability of MFQ to inhibit currents associated with Cx26-N14K could suggest a binding site in the vicinity of this residue in the cytoplasmic end of the channel pore. Although we present no direct evidence for this hypothesis, it is in agreement with previous mechanistic descriptions of connexin50 inhibition by a quaternary derivative of quinine, N-benzylquininium (Rubinos *et al.*, 2012). The absence of MFQ activity on Cx26-A88V, taken together with its atypical position in the second transmembrane domain, implies that divergent triggers of aberrant hemichannel behavior exist. In the case of Cx26-A88V and -N14K, an alternate inhibitor that is capable of pore block may be necessary to reduce open-channel dwell times. Owing to the size of the hemichannel pore (15–40 Å) (Maeda *et al.*, 2009), this strategy would require a larger molecule.

Extracellular Zn^{++} suppressed hemichannel activities for seven KID-causing Cx26 mutants

A limitation of quinine-family connexin inhibitors is their failure to distinguish between junctional and nonjunctional channel configurations. Divalent cations inhibit connexin channels and have been shown to act at the extracellular aspect of the pore to promote loop gating (Verselis and Srinivas, 2008). Robust gap-junctional conductances are routinely measured from cell pairs in the presence of extracellular Ca^{++}, indicating that binding of ions likely occurs at sites that are only accessible in undocked hemichannels. We recorded hemichannel currents from

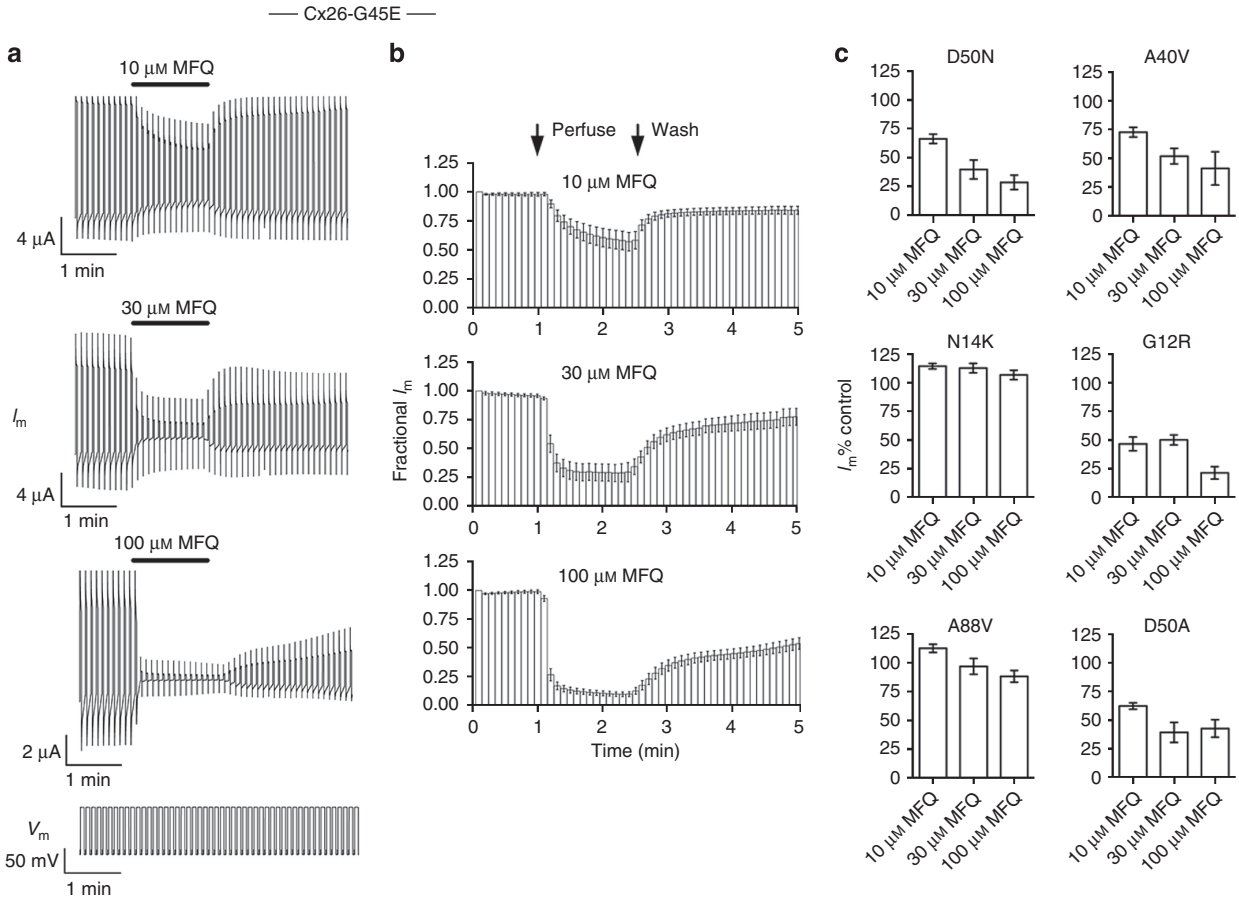

Figure 3. Mefloquine (MFQ) attenuated keratitis–ichthyosis–deafness-associated Cx26 hemichannel currents in a concentration-dependent and mutant-selective manner. (**a**) Voltage-clamp recordings for three cells expressing Cx26-G45E showed an increasing magnitude of membrane current (I_m) inhibition with 10, 30, and 100 μM MFQ. (**b**) Mean MFQ response characteristics across Cx26-G45E-expressing cells showed that membrane current, plotted as a fraction of the starting value, decreased by >25%, >50%, and >75% upon exposure to 10 ($N=5$), 30 ($N=5$), and 100 μM ($N=10$) MFQ, respectively. (**c**) Effect of 10, 30, and 100 μM MFQ perfusion on cells injected with Cx26-D50N, -A40V, -N14K, -G12R, -A88V, and -D50A. Bars represent the mean membrane current in the presence of the inhibitor as a percentage of the pre-drug value ($N=5$). Data are means ± SEM.

single *Xenopus* oocytes expressing Cx26-G45E in the presence and absence of 1, 10, and 100 μM extracellular Zn^{++}. Oocytes injected with H_2O passed negligible current, again providing a negative control. Those expressing Cx26-G45E showed large fluxes, as previously documented. Addition of Zn^{++} to the extracellular milieu caused membrane currents to diminish in a dose-dependent manner (Figure 4a). Mean currents were plotted as a function of membrane potential for each recording condition to facilitate comparison of current–voltage relationships (Figure 4b). Massive outward currents associated with Cx26-G45E were progressively reduced with 1, 10, and 100 μM Zn^{++} at all tested voltages. The degree of inhibition was quantified by perfusion of single cells during a paradigm of serial +100-mV pulses. For cells expressing Cx26-G45E, 73 ± 2.6% ($N=5$), 29 ± 2.1% ($N=5$), and 12 ± 3.9% ($N=5$) of the initial current persisted after 1.5 minutes of 1, 10, and 100 μM Zn^{++}, respectively (Figure 4c, extrapolated $IC_{50} \sim 3$ μM).

Zn^{++} inhibitory testing was repeated at 10 and 100 μM for Cx26-D50N, -A40V, -N14K, -G12R, -A88V, and -D50A (Figure 4c). Hemichannel activity was largely preserved in the presence of 10 μM Zn^{++}; only Cx26-G12R channels were >50% inhibited. Conversely, all mutant forms displayed >50% mean suppression at 10-fold higher Zn^{++} concentration. Notably, as with Cx26-G45E, 100 μM Zn^{++} abolished the membrane current associated with Cx26-A40V, -G12R, and -N14K by >80%. Together, these data support the use of Zn^{++} as another possible inhibitor to appraise the pathogenicity of hemichannels in KID syndrome.

In vitro expression of KID-associated mutant hemichannels causes cellular dysfunction and accelerated death that can be rescued by high extracellular calcium (Stong *et al.*, 2006; Lee *et al.*, 2009; Mhaske *et al.*, 2013). Constitutively active or "leaky" hemichannels may deplete the cells of important metabolites, such as ATP and cAMP, with deleterious consequences. In addition, changes in hemichannel calcium permeability have been clearly demonstrated for two mutations, Cx26-A40V and -G45E, suggesting that dysregulated hemichannels may provide a route for excessive entry of calcium (Sanchez *et al.*, 2010). Resulting imbalances in

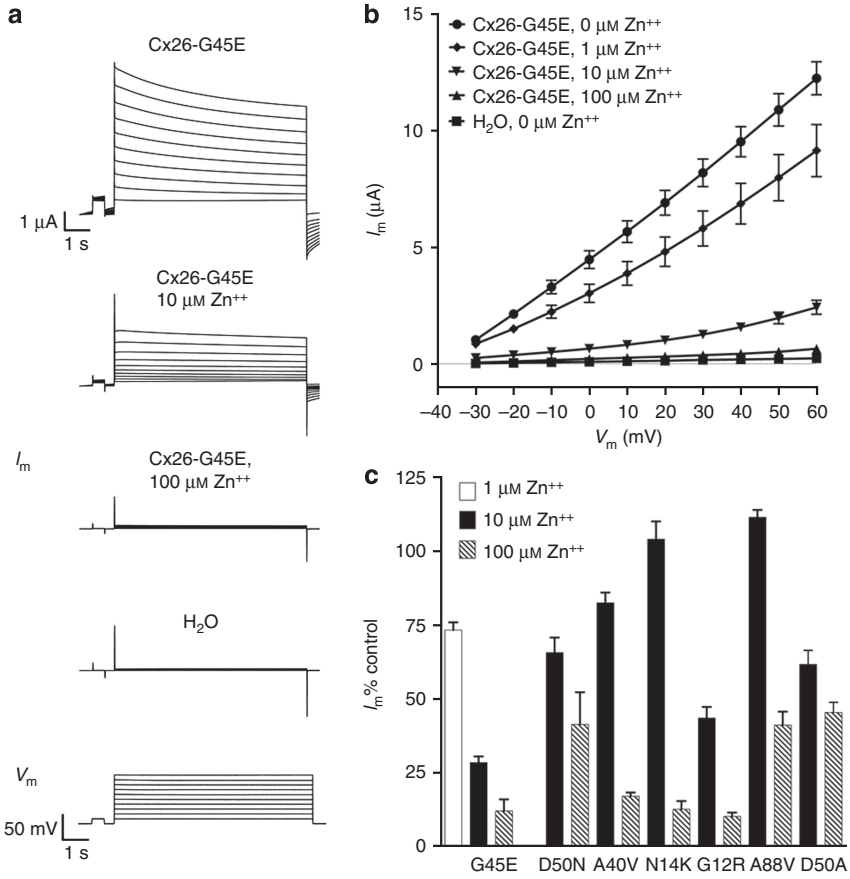

Figure 4. Extracellular zinc (Zn^{++}) reduced hemichannel currents mediated by keratitis–ichthyosis–deafness-causing Cx26 mutations. (**a**) Representative current (I_m) traces corresponding to a single Cx26-G45E-expressing cell recorded in the presence of 0, 10, and 100 μM Zn^{++}. An H_2O-injected control cell is shown for comparison. (**b**) Mean currents plotted against membrane potential (V_m) illustrated current–voltage relationships. Control cells showed negligible current ($N = 10$). Whole-cell currents observed in Cx26-G45E oocytes ($N = 16$) were inhibited by the addition of 1 ($N = 5$), 10 ($N = 5$), and 100 μM ($N = 5$) Zn^{++} to the medium. (**c**) Concentration-dependent effects of Zn^{++} perfusion in cells expressing Cx26-G45E, -D50N, -A40V, -N14K, -G12R, -A88V, and -D50A. Bars represent the mean current as a percentage of the pre-drug value for five cells. Data are means ± SEM.

intracellular–extracellular ionic gradients may disrupt paracrine signaling pathways or cause injurious osmotic pressures. Exogenous extracellular supply of a divalent cation, such as Zn^{++}, may reinforce an important mode of endogenous hemichannel regulation to prevent loss of cellular viability and tissue integrity.

MFQ inhibited elevated Cx26-G45E hemichannel currents in primary murine keratinocytes

A mouse model of KID syndrome has previously been developed by inducible epidermal expression of the human Cx26-G45E coding sequence (Mese *et al.*, 2011). Animals harboring Cx26-G45E experience epidermal pathology consistent with clinical reports describing human KID syndrome patients (Sbidian *et al.*, 2010; Koppelhus *et al.*, 2011; Mese *et al.*, 2011). Specifically, the phenotype manifests as diffuse erythrokeratoderma with profound epidermal thickening and scaling (Figure 5a). The design strategy featured bicistronic inclusion of the excitatory green fluorescent protein in the founder construct and backcrossing into a hairless strain (Figure 5b) to allow for visualization of affected tissue by *in vivo* fluorescence imaging (Figure 5c). Keratinocytes isolated from excised lesions retained transgene expression, as evidenced by excitatory green fluorescent protein signal, for several hours *ex vivo* (Figure 5d). We sought to substantiate the effectiveness of MFQ at suppressing Cx26-G45E membrane currents by whole-cell patch-clamp analysis of freshly isolated transgenic keratinocytes. G45E-Cx26 keratinocytes, identified by excitatory green fluorescent protein signature, showed high macroscopic membrane currents that were suppressed by 100 μM MFQ at all tested membrane potentials. Keratinocytes isolated from control littermates lacking Cx26-G45E were used to gauge the basal membrane current contributed by other voltage-activated channels present in the primary cells (Figure 5e). Cx26-G45E keratinocytes were previously shown to have significantly increased cell size by histological examination (Mese *et al.*, 2011). To account for this, cell membrane capacitance was measured to estimate cell surface area and used to compute current density before plotting the aggregate data as a function of membrane potential (Figure 5f). Control keratinocytes possessed modest membrane currents for potentials ranging

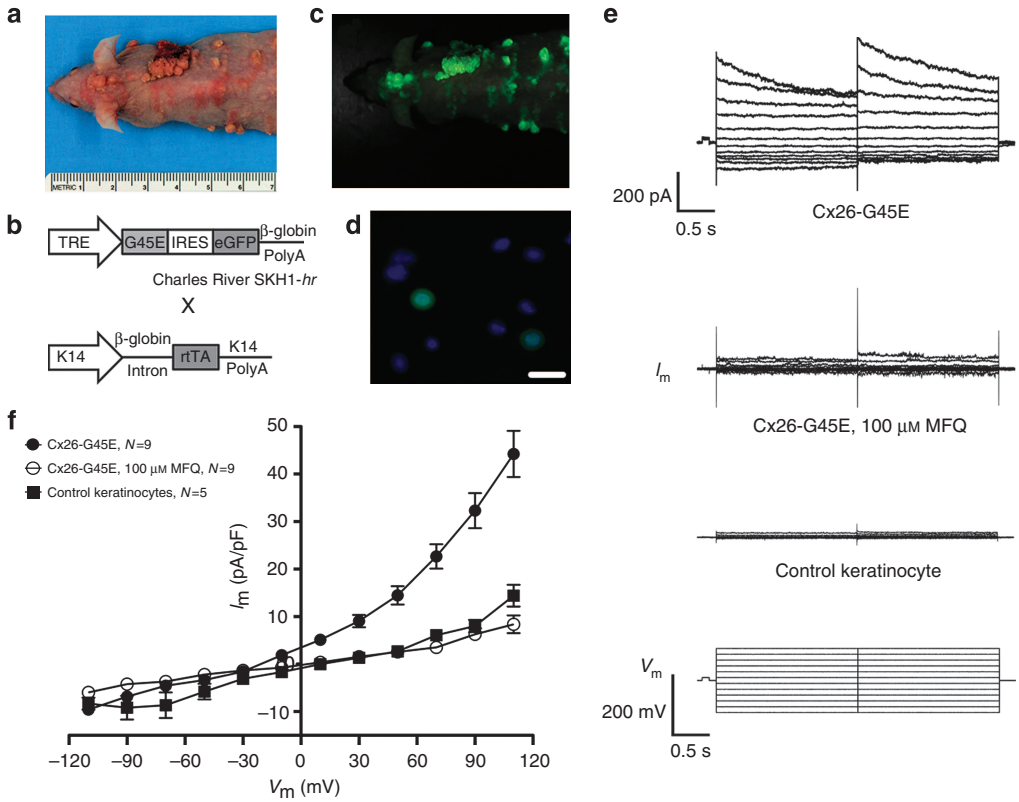

Figure 5. Mefloquine inhibited hemichannel activity in transgenic Cx26-G45E primary keratinocytes. (**a**, **b**) Cx26-G45E mice recapitulate the epidermal pathology of keratitis–ichthyosis–deafness syndrome using inducible tissue-specific expression of Cx26-G45E and excitatory green fluorescent protein (eGFP) in a hairless background. (**c**) *In vivo* fluorescence imaging demonstrated spatial correlation of fluorescence with skin lesions. (**d**) Keratinocytes isolated from Cx26-G45E lesions retained eGFP expression, facilitating their identification for patch-clamp electrophysiology (bar = 10 μm). (**e**) Whole-cell membrane currents (I_m) were recorded by patch-clamp electrophysiology. Nominal currents were observed in control keratinocytes. (**f**) Current density plotted against membrane potential (V_m) showed that large macroscopic currents were elicited from Cx26-G45E cells ($N = 9$) that were diminished by the addition of 100 μM mefloquine ($N = 9$) to levels resembling control cells ($N = 5$). Data are means ± SEM.

from −110 to +110 mV. Cx26-G45E keratinocytes passed substantially higher currents, particularly at depolarizing voltages. Rerecording in the presence of 100 μM MFQ reduced membrane currents to levels at or below control. The data indicate that 100 μM MFQ is adequate to eliminate Cx26-G45E hemichannel activity in a mammalian system of higher complexity and physiological relevance. MFQ has been observed to additionally block voltage-gated L-type calcium channels, Kir6.2 and KvLQT1 potassium channels, volume-regulated and calcium activated chloride channels, and pannexins (Gribble *et al.*, 2000; Maertens *et al.*, 2000; Kang *et al.*, 2001; Traebert *et al.*, 2004; Suadicani *et al.*, 2006; Verselis and Srinivas, 2013). Optimization of the molecular structure to enrich sensitivity for Cx26 and/or decrease affinity for other targets may be possible through medicinal chemistry techniques (Wermuth, 2004). Nevertheless, MFQ can potently inhibit Cx26-G45E hemichannels. Minimally, this provides an agent to further structure–function analyses to elucidate the molecular bases of errors in gating and permeation that accompany mutations. Importantly, MFQ and related hemichannel inhibitors may have therapeutic utility in KID syndrome.

In summary, we show two *in vitro* functional assays supporting the use of MFQ and extracellular Zn^{++} as hemichannel inhibitors to study Cx26 mutants linked to KID syndrome. Extracellular Zn^{++} demonstrated marginally higher potency, as well as fuller coverage of the Cx26 hemichannel mutant forms considered. Furthermore, Zn^{++} may represent a gap junction–sparing inhibitor that is useful for isolating the explicit functions of hemichannels that relate to homeostatic maintenance. Unfortunately, the pervasive involvement of divalent cations in cellular processes would likely invite a plethora of off-target secondary effects that may preclude fruitful testing in animal models.

MFQ may provide a viable small-molecule inhibitor for certain Cx26 mutants, including the lethal Cx26-G45E, particularly given the paucity of reagents with higher specificity/selectivity. MFQ has been reported to inhibit only one connexin isoform colocalizing with Cx26 in the epidermis, Cx43 (Cruikshank *et al.*, 2004). Loss of cellular coupling by Cx43 causes the developmental ectodermal disorder oculodentodigital dysplasia, which involves little disturbance of epidermal proliferation/differentiation (Jamsheer *et al.*, 2014). Moreover, a distinct set of Cx26 mutations causing palmoplantar keratoderma are thought to operate through transdominant inhibition of WT Cx43 (Rouan *et al.*, 2001). These mutations cause hyperkeratosis that is confined to

palmar/plantar skin, indicating that other connexin and nonconnexin membrane channels may be capable of compensating for deficiencies in Cx43 function elsewhere (Richard *et al.*, 1998). An overlap in gap-junction and hemichannel blocking activity remains the primary drawback associated with MFQ. However, defects in Cx26 gap-junctional communication do not appear to be causative of epidermal pathologies. Cx26 mutations causing KID syndrome have proven to be capricious with regard to their retention or deficiency of gap-junction functionality. For example, expression of Cx26-G45E and -N14K in cell pairs leaves gap-junctional conductance unaffected relative to WT (gating is altered, however), whereas active coupling is not detected for Cx26-G12R and -D50N (Gerido *et al.*, 2007; Lee *et al.*, 2009). The clearest indication that the native function of Cx26 is not essential in the epidermis stems from the absence of cutaneous abnormalities in patients with autosomal recessive nonsyndromic hearing loss, which is predominantly due to loss of Cx26 function (White, 2000; Zhao *et al.*, 2006). The apparent apathy of the epidermis to Cx26 gap-junction functional status favors the use of MFQ in exploring the pathological implications of excessive hemichannel currents.

Whether alterations in Cx26 hemichannel patency and/or permeability are sufficient to upset epidermal homeostasis in KID syndrome remains to be definitively shown. Hemichannels are speculated to participate in delicate paracrine signaling, which may involve the extracellular release of ATP (Cotrina *et al.*, 1998; Kang *et al.*, 2008), glutamate (Ye *et al.*, 2003), NAD^+ (Bruzzone *et al.*, 2001), and prostaglandins (Jiang and Cherian, 2003). Connexin-specific inhibitors, with subtype-selectivity and high affinity for mutant forms causing human genetic diseases, are needed to evaluate hypotheses formulated from *in vitro* functional studies. The use of currently available inhibitors in animal models will help clarify a physiological niche for unapposed hemichannels in numerous tissue systems and may offer novel therapeutic strategies for gain-of-function genetic disorders.

MATERIALS AND METHODS

Molecular cloning

Human WT and mutant Cx26 were cloned into the *Bam*HI restriction site of the pCS2+ expression vector (Turner and Weintraub, 1994) for functional assays in *Xenopus laevis* oocytes. Cx26-G45E, -D50N, -G12R, -N14K, -A88V, and -D50A were prepared from the WT template by site-directed mutagenesis using overlap extension PCR (Horton *et al.*, 1990), as previously described (Gerido *et al.*, 2007; Lee *et al.*, 2009; Mhaske *et al.*, 2013). Cx26-A40V was directly amplified from patient genomic DNA, as previously described (Montgomery *et al.*, 2004).

In vitro transcription and oocyte microinjection

Plasmids were linearized by NotI digestion and transcribed using the SP6 mMessage mMachine (Ambion, Austin, TX) to yield cRNAs. The Stony Brook University IACUC approved oocyte removal from *Xenopus*. Adult females were anesthetized with ethyl 3-aminobenzoate methanesulfonate, and ovarian lobes were surgically excised. Oocyte lobes were digested in 7.5 mg ml^{-1} collagenase B and 5.0 mg ml^{-1} hyaluronidase in modified Barth's medium without Ca^{++} for 15 minutes at 37 °C with constant shaking. Stage V–VI oocytes were separated and injected with 10 ng of an antisense morpholino oligonucleotide to Cx38 (Barrio *et al.*, 1991; Bruzzone *et al.*, 1993), to eliminate endogenous connexin. Oocytes were injected with WT Cx26, Cx26-G45E, -D50N, -A40V, -A88V, -G12R, -D50A, and -N14K cRNA transcripts, or H_2O as a negative control and cultured in modified Barth's medium supplemented with 4 mM $CaCl_2$ for 15–18 hours before electrophysiological assay.

Western blotting

Oocytes were homogenized in 1 ml of buffer containing 5 mM Tris, pH 8.0, 5 mM EDTA, and protease inhibitors (Roche diagnostics, Indianapolis, IN) by mechanical passage through a series of needles of diminishing size (White *et al.*, 1992). Membranes were pelleted by centrifugation at 100,000 *g* for 30 minutes, resuspended in SDS sample buffer (2 µl per oocyte), separated on 12% SDS gels, and transferred to nitrocellulose membranes. Blots were blocked with 5% milk in 1x tris-buffered saline/0.1% tween20 for 1 hour at room temperature and probed with a polyclonal rabbit anti-Cx26 antibody (Invitrogen, Carlsbad, CA) at a 1:1,000 dilution and subsequently incubated with a horseradish peroxidase–conjugated anti-rabbit secondary antibody (Jackson ImmunoResearch, West Grove, PA) at 1:5,000 dilution. For loading control, blots were washed, reprobed with a monoclonal mouse β-actin antibody (Abcam, Cambridge, MA), and incubated with a horseradish peroxidase–conjugated anti-mouse secondary antibody (GE Healthcare Biosciences, Pittsburgh, PA). Band densities were quantified using the ImageJ software.

Drugs

Quinine-family small molecules included MFQ (([R*,S*]-[2,8-Bis-trifluoromethyl-quinolin-4-yl]-piperidin-2-yl-methanol hydrochloride), QU020 ([2,8-Bis-trifluoromethyl-quinolin-4-yl]-pyridin-2-yl-methanone), QU021 (2,8-Bis[trifluoromethyl]-4-quinolyl[1-oxypyrid-2-yl] methane), QU022 (4-Chloro-2-trichloromethyl-quinoline), and QU026 ([2,8-Bis-trifluoromethyl-quinolin-4-yl]-pyridin-2-yl-methanol)), and were acquired from Bioblocks (San Diego, CA). Drugs were solubilized in DMSO at a stock concentration of 100 mM and stored at −20 °C.

Recording of hemichannel currents

Recordings of hemichannel currents were acquired from single oocytes using a GeneClamp 500 amplifier controlled by a PC-compatible computer through a Digidata 1440A interface (Axon instruments, Foster City, CA). Stimulus and data collection paradigms were programmed with pClamp 10.2 (Axon Instruments). Current and voltage electrodes (1.5 mm diameter glass, World Precision Instruments, Sarasota, FL) were pulled to a resistance of 1-2 MΩ on a vertical puller (Narishige, Tokyo, Japan) and filled with a conducting solution containing 3 M KCl, 10 mM EGTA, and 10 mM HEPES, pH 7.4. Whole-cell current traces were obtained by initial clamping at −40 mV and subsequent 5- to 8-second depolarizing pulses spanning −30 to +60 mV in 10-mV increments (Lee *et al.*, 2009). Pharmacologic inhibitor compounds were tested during a 50-sweep series of 5-second 100-mV depolarizations from the −40 mV holding potential over a 5-minute experimental duration. Recordings were initiated by perfusion with modified Barth's medium lacking Ca^{++} for a 10-pulse period to ensure minimal clamp leakage and stability of

the steady-state membrane current. Small-molecule inhibitors or ionic salts ($ZnSO_4$) were then introduced using a three-way valve to rapidly exchange bathing solutions in a custom 0.5-ml chamber for 15 voltage pulses. During the final 25-pulse period, the inhibitor solution was flushed out with modified Barth's medium lacking Ca^{++} to assess reversibility. Whole-cell membrane current corresponding to each voltage pulse was extracted from raw data and normalized to the starting current for examination of the fractional change upon perfusion.

Isolation of transgenic Cx26-G45E keratinocytes

Murine keratinocytes with transgenic expression of human Cx26-G45E were isolated from epidermal tissue, as previously described (Mese *et al.*, 2011). KID lesions were induced in animals by 2 weeks of doxycycline-supplemented diet (200 mg kg^{-1}). Lesion severity was assessed by *in vivo* detection of excitatory green fluorescent protein in a Maestro small-animal imaging system (Cri, Woburn, MA). After euthanasia, 3–5 mm skin lesions comprising the epidermis and dermis were resected and cells were isolated for short-term culture (Lichti *et al.*, 2008). Samples were floated in 0.25% trypsin at 37 °C for 45 minutes, mechanically minced, passed through a 100-μm cell strainer, and plated on 12-mm glass coverslips coated with 40 μM poly-D-lysine hydrobromide to facilitate rapid attachment. Primary cells were cultured in regular medium supplemented with 0.2 mM $CaCl_2$ for 2 hours at 37 °C and 5% CO_2 before using for immunocytochemistry or patch-clamp electrophysiology. The Stony Brook University IACUC approved all mouse procedures. Keratinocytes were fixed with 1% paraformaldehyde in phosphate-buffered saline for 1 hour, and then blocked and permeabilized with 5% bovine serum albumin in phosphate-buffered saline plus 0.1% Triton X-100 for 30 minutes. Coverslips were mounted on slides using Vectashield with DAPI (Vector Laboratories, Burlingame, CA). Slides were viewed on a BX51 microscope and photographed with a DP72 digital camera (Olympus, Lake Success, NY).

Patch-clamp electrophysiology

Primary murine epidermal keratinocytes were used for whole-cell patch-clamp at room temperature, as previously described (Mese *et al.*, 2011). To begin each experiment, cells were clamped at 0 mV and subsequently stepped from −110 to +110 mV in 20-mV increments. After the initial set of hemichannel current recordings, inhibitor effects were tested by perfusing dishes with small molecules (MFQ/QU0) diluted in Tyrode's solution, and rerecording within 30–90 seconds of medium exchange.

CONFLICT OF INTEREST

The authors state no conflict of interest.

ACKNOWLEDGMENTS

This work was supported by National Institutes of Health grant R01 AR59505 (TWW) from the National Institute of Arthritis and Musculoskeletal and Skin Diseases.

REFERENCES

Barrio LC, Suchyna T, Bargiello T *et al.* (1991) Gap junctions formed by connexins 26 and 32 alone and in combination are differently affected by applied voltage. *Proc Natl Acad Sci USA* 88:8410–4

Bruzzone R, Haefliger JA, Gimlich RL *et al.* (1993) Connexin40, a component of gap junctions in vascular endothelium, is restricted in its ability to interact with other connexins. *Mol Biol Cell* 4:7–20

Bruzzone R, White TW, Paul DL (1996) Connections with connexins: the molecular basis of direct intercellular signaling. *Eur J Biochem* 238:1–27

Bruzzone S, Guida L, Zocchi E *et al.* (2001) Connexin 43 hemi channels mediate Ca2 + -regulated transmembrane NAD + fluxes in intact cells. *FASEB J* 15:10–2

Bukauskas FF, Peracchia C (1997) Two distinct gating mechanisms in gap junction channels: CO2-sensitive and voltage-sensitive. *Biophys J* 72:2137–42

Cotrina ML, Lin JH, Alves-Rodrigues A *et al.* (1998) Connexins regulate calcium signaling by controlling ATP release. *Proc Natl Acad Sci USA* 95:15735–40

Cruikshank SJ, Hopperstad M, Younger M *et al.* (2004) Potent block of Cx36 and Cx50 gap junction channels by mefloquine. *Proc Natl Acad Sci USA* 101:12364–9

DeVries SH, Schwartz EA (1992) Hemi-gap-junction channels in solitary horizontal cells of the catfish retina. *J Physiol* 445:201–30

Donnelly S, English G, de Zwart-Storm EA *et al.* (2012) Differential susceptibility of Cx26 mutations associated with epidermal dysplasias to peptidoglycan derived from *Staphylococcus aureus* and *Staphylococcus epidermidis*. *Exp Dermatol* 21:592–8

Ebihara L, Steiner E (1993) Properties of a nonjunctional current expressed from a rat connexin46 cDNA in *Xenopus* oocytes. *J Gen Physiol* 102:59–74

Gerido DA, DeRosa AM, Richard G *et al.* (2007) Aberrant hemichannel properties of Cx26 mutations causing skin disease and deafness. *Am J Physiol Cell Physiol* 293:C337–45

Gonzalez D, Gomez-Hernandez JM, Barrio LC (2006) Species specificity of mammalian connexin-26 to form open voltage-gated hemichannels. *FASEB J* 20:2329–38

Goodenough DA, Paul DL (2009) Gap junctions. *Cold Spring Harb Perspect Biol* 1:a002576

Gribble FM, Davis TM, Higham CE *et al.* (2000) The antimalarial agent mefloquine inhibits ATP-sensitive K-channels. *Br J Pharmacol* 131:756–60

Griffith AJ, Yang Y, Pryor SP *et al.* (2006) Cochleosaccular dysplasia associated with a connexin 26 mutation in keratitis-ichthyosis-deafness syndrome. *Laryngoscope* 116:1404–8

Haruna K, Suga Y, Oizumi A *et al.* (2010) Severe form of keratitis-ichthyosis-deafness (KID) syndrome associated with septic complications. *J Dermatol* 37:680–2

Horton RM, Cai ZL, Ho SN *et al.* (1990) Gene splicing by overlap extension: tailor-made genes using the polymerase chain reaction. *Biotechniques* 8:528–35

Jamsheer A, Sowinska-Seidler A, Socha M *et al.* (2014) Three novel GJA1 missense substitutions resulting in oculo-dento-digital dysplasia (ODDD)—Further extension of the mutational spectrum. *Gene* 539:157–61

Janecke AR, Hennies HC, Gunther B *et al.* (2005) GJB2 mutations in keratitis-ichthyosis-deafness syndrome including its fatal form. *Am J Med Genet A* 133A:128–31

Jiang JX, Cherian PP (2003) Hemichannels formed by connexin 43 play an important role in the release of prostaglandin E(2) by osteocytes in response to mechanical strain. *Cell Commun Adhes* 10:259–64

Jonard L, Feldmann D, Parsy C *et al.* (2008) A familial case of Keratitis-Ichthyosis-Deafness (KID) syndrome with the GJB2 mutation G45E. *Eur J Med Genet* 51:35–43

Kang J, Chen XL, Wang L *et al.* (2001) Interactions of the antimalarial drug mefloquine with the human cardiac potassium channels KvLQT1/minK and HERG. *J Pharmacol Exp Ther* 299:290–6

Kang J, Kang N, Lovatt D *et al.* (2008) Connexin 43 hemichannels are permeable to ATP. *J Neurosci* 28:4702–11

Koppelhus U, Tranebjaerg L, Esberg G *et al.* (2011) A novel mutation in the connexin 26 gene (GJB2) in a child with clinical and histological features of keratitis-ichthyosis-deafness (KID) syndrome. *Clin Exp Dermatol* 36:142–8

Kronengold J, Srinivas M, Verselis VK (2012) The N-terminal half of the connexin protein contains the core elements of the pore and voltage gates. *J Membr Biol* 245:453–63

Kronengold J, Trexler EB, Bukauskas FF *et al.* (2003) Pore-lining residues identified by single channel SCAM studies in Cx46 hemichannels. *Cell Commun Adhes* 10:193–9

Lee JR, Derosa AM, White TW (2009) Connexin mutations causing skin disease and deafness increase hemichannel activity and cell death when expressed in *Xenopus* oocytes. *J Invest Dermatol* 129:870–8

Li Z, Yan Y, Powers EA *et al.* (2003) Identification of gap junction blockers using automated fluorescence microscopy imaging. *J Biomol Screen* 8:489–99

Lichti U, Anders J, Yuspa SH (2008) Isolation and short-term culture of primary keratinocytes, hair follicle populations and dermal cells from newborn mice and keratinocytes from adult mice for in vitro analysis and for grafting to immunodeficient mice. *Nat Protoc* 3:799–810

Maeda S, Nakagawa S, Suga M *et al.* (2009) Structure of the connexin 26 gap junction channel at 3.5 A resolution. *Nature* 458:597–602

Maertens C, Wei L, Droogmans G *et al.* (2000) Inhibition of volume-regulated and calcium-activated chloride channels by the antimalarial mefloquine. *J Pharmacol Exp Ther* 295:29–36

Malchow RP, Qian H, Ripps H (1993) Evidence for hemi-gap junctional channels in isolated horizontal cells of the skate retina. *J Neurosci Res* 35:237–45

Mazereeuw-Hautier J, Bitoun E, Chevrant-Breton J *et al.* (2007) Keratitis-ichthyosis-deafness syndrome: disease expression and spectrum of connexin 26 (GJB2) mutations in 14 patients. *Br J Dermatol* 156:1015–9

Mese G, Sellitto C, Li L *et al.* (2011) The Cx26-G45E mutation displays increased hemichannel activity in a mouse model of the lethal form of keratitis-ichthyosis-deafness syndrome. *Mol Biol Cell* 22:4776–86

Mhaske PV, Levit NA, Li L *et al.* (2013) The human Cx26-D50A and Cx26-A88V mutations causing keratitis-ichthyosis-deafness syndrome display increased hemichannel activity. *Am J Physiol Cell Physiol* 304:C1150–8

Montgomery JR, White TW, Martin BL *et al.* (2004) A novel connexin 26 gene mutation associated with features of the keratitis-ichthyosis-deafness syndrome and the follicular occlusion triad. *J Am Acad Dermatol* 51:377–82

Pfenniger A, Wohlwend A, Kwak BR (2011) Mutations in connexin genes and disease. *Eur J Clin Invest* 41:103–16

Picoli C, Nouvel V, Aubry F *et al.* (2012) Human connexin channel specificity of classical and new gap junction inhibitors. *J Biomol Screen* 17:1339–47

Richard G (2005) Connexin disorders of the skin. *Clin Dermatol* 23:23–32

Richard G, Rouan F, Willoughby CE *et al.* (2002) Missense mutations in GJB2 encoding connexin-26 cause the ectodermal dysplasia keratitis-ichthyosis-deafness syndrome. *Am J Hum Genet* 70:1341–8

Richard G, White TW, Smith LE *et al.* (1998) Functional defects of Cx26 resulting from a heterozygous missense mutation in a family with dominant deaf-mutism and palmoplantar keratoderma. *Hum Genet* 103:393–9

Ripps H, Qian H, Zakevicius J (2004) Properties of connexin26 hemichannels expressed in *Xenopus* oocytes. *Cell Mol Neurobiol* 24:647–65

Rouan F, White TW, Brown N *et al.* (2001) Trans-dominant inhibition of connexin-43 by mutant connexin-26: implications for dominant connexin disorders affecting epidermal differentiation. *J Cell Sci* 114:2105–13

Rubinos C, Sanchez HA, Verselis VK *et al.* (2012) Mechanism of inhibition of connexin channels by the quinine derivative N-benzylquininium. *J Gen Physiol* 139:69–82

Sanchez HA, Mese G, Srinivas M *et al.* (2010) Differentially altered Ca2+ regulation and Ca2+ permeability in Cx26 hemichannels formed by the A40V and G45E mutations that cause keratitis ichthyosis deafness syndrome. *J Gen Physiol* 136:47–62

Sbidian E, Feldmann D, Bengoa J *et al.* (2010) Germline mosaicism in keratitis-ichthyosis-deafness syndrome: pre-natal diagnosis in a familial lethal form. *Clin Genet* 77:587–92

Scott CA, Kelsell DP (2011) Key functions for gap junctions in skin and hearing. *Biochem J* 438:245–54

Skinner BA, Greist MC, Norins AL (1981) The keratitis, ichthyosis, and deafness (KID) syndrome. *Arch Dermatol* 117:285–9

Srinivas M, Hopperstad MG, Spray DC (2001) Quinine blocks specific gap junction channel subtypes. *Proc Natl Acad Sci USA* 98:10942–7

Srinivas M, Spray DC (2003) Closure of gap junction channels by arylamino-benzoates. *Mol Pharmacol* 63:1389–97

Stong BC, Chang Q, Ahmad S *et al.* (2006) A novel mechanism for connexin 26 mutation linked deafness: cell death caused by leaky gap junction hemichannels. *Laryngoscope* 116:2205–10

Suadicani SO, Brosnan CF, Scemes E (2006) P2X7 receptors mediate ATP release and amplification of astrocytic intercellular Ca2+ signaling. *J Neurosci* 26:1378–85

Tang Q, Dowd TL, Verselis VK *et al.* (2009) Conformational changes in a pore-forming region underlie voltage-dependent ''loop gating'' of an unapposed connexin hemichannel. *J Gen Physiol* 133:555–70

Traebert M, Dumotier B, Meister L *et al.* (2004) Inhibition of hERG K+ currents by antimalarial drugs in stably transfected HEK293 cells. *Eur J Pharmacol* 484:41–8

Turner DL, Weintraub H (1994) Expression of achaete-scute homolog 3 in *Xenopus* embryos converts ectodermal cells to a neural fate. *Genes Dev* 8:1434–47

Verselis VK, Ginter CS, Bargiello TA (1994) Opposite voltage gating polarities of two closely related connexins. *Nature* 368:348–51

Verselis VK, Srinivas M (2008) Divalent cations regulate connexin hemichannels by modulating intrinsic voltage-dependent gating. *J Gen Physiol* 132:315–27

Verselis VK, Srinivas M (2013) Connexin channel modulators and their mechanisms of action. *Neuropharmacology* 75:517–24

Verselis VK, Trelles MP, Rubinos C *et al.* (2009) Loop gating of connexin hemichannels involves movement of pore-lining residues in the first extracellular loop domain. *J Biol Chem* 284:4484–93

Weingart R, Bukauskas FF (1998) Long-chain n-alkanols and arachidonic acid interfere with the Vm-sensitive gating mechanism of gap junction channels. *Pflugers Arch* 435:310–9

Wermuth CG (2004) Selective optimization of side activities: another way for drug discovery. *J Med Chem* 47:1303–14

White TW (2000) Functional analysis of human Cx26 mutations associated with deafness. *Brain Res Brain Res Rev* 32:181–3

White TW, Bruzzone R, Goodenough DA *et al.* (1992) Mouse Cx50, a functional member of the connexin family of gap junction proteins, is the lens fiber protein MP70. *Mol Biol Cell* 3:711–20

Ye ZC, Wyeth MS, Baltan-Tekkok S *et al.* (2003) Functional hemichannels in astrocytes: a novel mechanism of glutamate release. *J Neurosci* 23:3588–96

Zhao HB, Kikuchi T, Ngezahayo A *et al.* (2006) Gap junctions and cochlear homeostasis. *J Membr Biol* 209:177–86